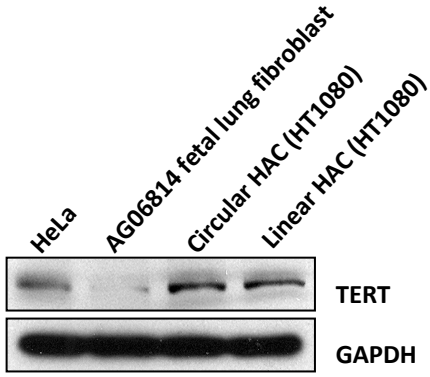

Figure S1 Western blot analysis of telomerase protein (hTERT) in human fibrosarcoma HT1080 cell line.

A

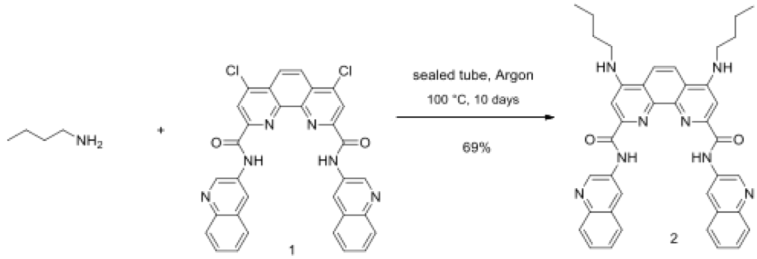

A sealed tube containing the dichloro derivative 1 (66.0mg, 0.112mmol, 1.0eq) and Butylamine (1.5mL, 15.18mmol, 135.0eq) under argon was heated to 100°C for 10 days and formation of a yellow precipitate floating in an orange solution was observed. After addition of H_2O (10mL) the solid was filtrated on Nylon membrane leading to the diamino product 2 obtained as a yellow solid (51.0mg, **69%**). ^{1}H NMR (300 MHz, [D_6]DMSO) : d = 11.73 (s, 2H), 9.66 (d, *J*= 3.0 Hz, 2H), 9.08 (d, *J*= 3.0Hz, 2H), 8.35 (s, 2H), 8.06 (m, 4H), 7.76-7.63 (m, 6H), 7.56 (s, 2H), 3.46 (m, 4H), 1.78 (m, 4H), 1.53 (m, 4H), 1.02 (t, *J*= 7.3Hz, 6H). ESI-MS $C_{40}H_{38}N_8O_2$ Exact Mass : 662.31 ; $[M+H]^+$: 663.1

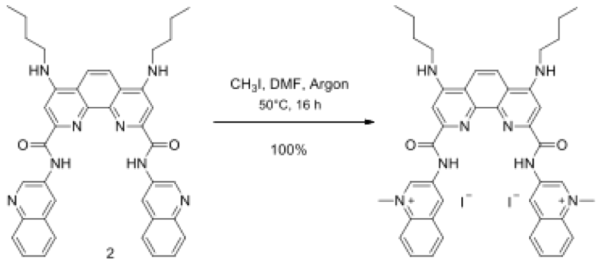

PhenDC3 Bisalk1

To the solution of compound 2 (30.0mg, 0.045mmol, 1.0eq) in DMF (1.4mL) was added dropwise Methyl iodide (0.4mL, 6.425mmol, 141.0eq). The resulting reaction mixture was stirred at 50°C overnight. The precipitate was filtered off and dried with addition of Et_2O affording the expected product as a yellow-orange solid (49.0mg, **100%**).^{1}H NMR (300 MHz, [D_6]DMSO, 75°C) : d = 10.17 (s, 2H), 9.69 (s, 2H), 8.56-8.44 (m, 6H), 8.25 (m,2H), 8.06 (m, 2H), 7.67 (s, 2H), 4.73 (s, 6H), 2.59 (m, 2H), 1.83 (m, 4H), 1.56 (m, 4H), 1.04 (t, *J*= 7.3Hz, 6H). ESI-MS $C_{42}H_{44}I_2N_8O_2$: M = 946.17, m/z : 346.4 $[M+H]^+$

B

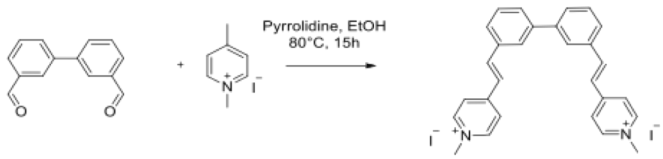

BisphenylV-Py

A mixture of [1,1'-Biphenyl]-3,3'-dicarboxaldehyde (210.2mg, 0.15mmol, 1.0 eq) and 1,4-dimethyl-pyridinium iodide (235.1mg, 0.30mmol, 2 eq.) was refluxed in ethanol (40 mL) in the presence of pyrrolidine (50 µL) for 2 h. The reaction mixture was filtered, washed with ethanol affording the expected product BisphenylV-py as a beige solid (80.0mg, 82%). ^{1}H NMR (300 MHz, DMSO) δ 8.89 (d, *J* = 6.5 Hz, 4H), 8.25 (d, *J* = 6.5 Hz, 4H), 8.17 – 8.07 (m, 4H), 7.84-7.77 (m, 4H), 7.72-7.62 (m, 4H), 4.27 (s, 6H). ^{13}C NMR (75 MHz, DMSO) δ 152.39, 145.23, 140.31, 135.93, 129.85, 128.75, 127.75, 126.27, 123.90, 123.60, 47.02. MS (ES+) : m/z 195.3 $[M-2I^-]^{2+}$.

C

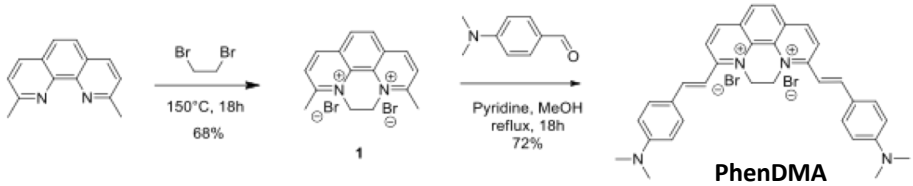

PhenDMA

Compound 1 (CAS 19934-04-4): Neocuproine (1.085 g, 5 mmol, 1 eq.) and dibromoethane (20 mL, 230 mmol, 46 eq.) were stirred at reflux for 8h. The reaction mixture was filtered and washed with chloroform to afford **1** in 68% yield (1.36 g, 34%) as an orange solid. ^{1}H NMR (300 MHz, D_2O) δ 9.27 (d, J= 8.7, 2H), 8.57 (s, 2H), 8.44 (d, J=8.7, 2H), 5.49 (s, 4H), 3.24 (6H); M(ESI^+) *m/z* 118.1

PhenDMA: A mixture of compound **1** (200 mg, 0.5 mmol, 1 eq) and dimethylaminobenzaldehyde (149 mg, 1,0 mmol, 2 eq) was refluxed in methanol (20 mL) for in the presence of pyridine (100 µL) for 18h. The mixture was cooled filtered and washed with ether to afford **PhenDMA** in 72% yield (240 mg, 0.36 mmol). ^{1}H NMR (300 MHz, DMSO) δ 8.96 (d, *J* = 9.2 Hz, 2H), 8.87 (d, *J* = 9.2 Hz, 2H), 8.49 (d, *J* = 15.2 Hz, 2H), 8.38 (s, 2H), 7.95 (d, *J* = 8.5 Hz, 4H), 7.69 (d, *J* = 15.2 Hz, 2H), 6.89 (d, *J* = 8.5 Hz, 4H), 5.38 (s, 4H), 3.13 (s, 12H) ; M(ESI^+) *m/z* 249.2; HRMS (ESI^+): m/z calcd for $[C_{34}H_{34}N_2]^+$ 498.2772; found 498.2765

D

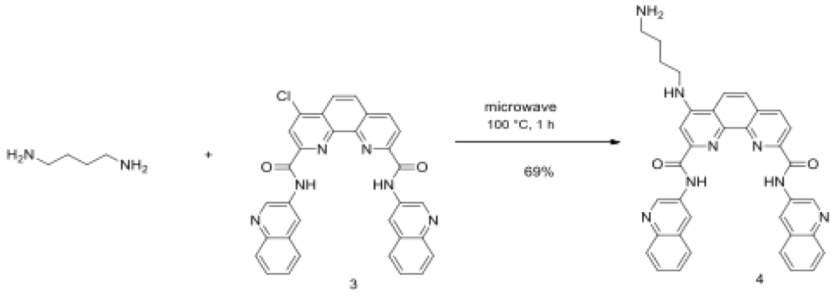

PhenDC3monochloro derivative 3 (80.0mg, 0.145mmol, 1.0eq) and 1,4-diaminobutane (2.0mL, 19.955mmol, 138.0eq) were heated to 100°C for 1h in a tube using *MW*. Upon addition of CH_3CN (80mL) a precipitate was formed. The solid was filtered, washed with CH_3CN and dried with Et_2O. Compound 4 was obtained as a clear yellow solid (60mg, **69%**). ^1H NMR (300 MHz, $[D_6]DMSO$) : d = 9.66 (m, 2H), 9.11 (dd, *J*= 3.0 Hz, *J*= 12Hz, 2H), 8.76 (d, *J*= 9Hz, 1H), 8.55 (m, 2H), 8.08 (m, 5H), 7.90 (s, 1H), 7.69 (m, 6H), 2.67 (t, *J*= 6Hz, 2H), 1.81 (m, 2H), 1.57 (m, 2H). ESI-MS $C_{36}H_{30}O_8N_2$: Exact mass 606.25 ; $[M+H]^+$: 607.2

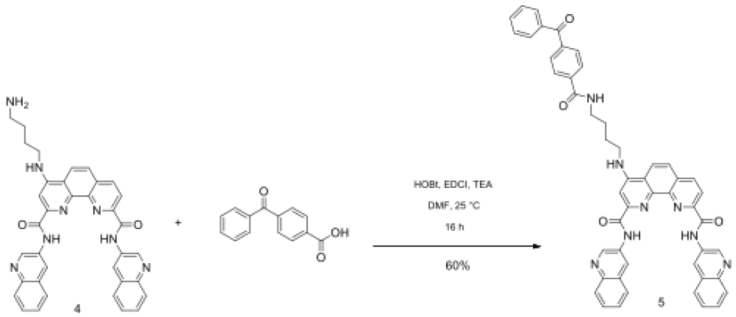

A mixture of compound 4 (49.0mg, 0.076mmol, 1.0eq), Benzoyl benzoic acid (17.2mg, 0.076mmol, 1.0eq), HOBt (4.1mg, 0.030mmol, 0.4eq), EDCI (11.8mg, 0.076mg, 1.0eq), TEA (0.026mL, 0.190mmol, 2.5eq) in dry DMF (1.5mL) was stirred overnight at room temperature protected from the light and under argon atmosphere for 16h. The reaction mixture was yellow and heterogeneous. Evaporation of DMF under reduced pressure led to a yellow solid residue which was purified by SiO_2 chromatography using DCM-MeOH 100-0 to 95-5. The expected product 5 was obtained as a yellow solid (37.0mg, **60%**).^1H NMR (300 MHz, $[D_6]DMSO$) : d = 11.80 (m, 2H), 9.67 (m, 2H), 9.12 (m, 2H), 8.78 (m, 2H), 8.59 (m, 2H), 8.13-7.99 (m, 7H), 7.79-7.65 (m, 10H), 7.54 (m, 2H), 3.55 (m,2H), 3.43 (m, 2H), 1.85(m, 4H). ESI-MS $C_{50}H_{38}N_8O_4$: Exact Mass 814.3 ; $[M+H]^+$: 815.5

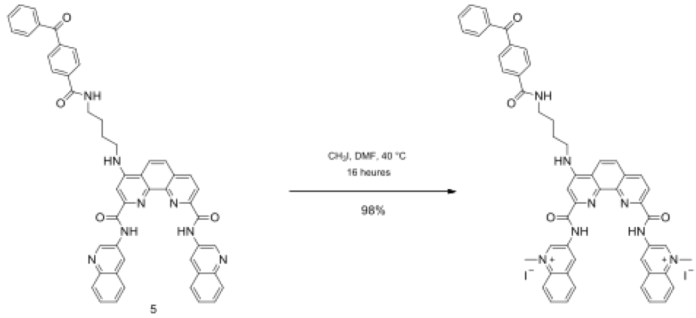

PhenDC3C4bn

To the solution of compound 5 (32.0mg, 0.390mmol, 1.0eq) in dry DMF (1.1mL) at 40°C under argon was added dropwise Methyl iodide (0.097mL, 1.57mmol, 40.0eq). The reaction mixture was stirred at 40°C for 36h in the dark. The initial orange solution became yellow and heterogeneous. DMF was evaporated to dryness and the resulting solid was taken up from Et_2O (2mL) and washed with it (4mL) and dried under vacuum. The expected product **PhenDC3 C4Bn** was obtained as a yellow solid (41.0mg, **95%**).^1H NMR (300 MHz, $[D_6]DMSO$) : d = 12.12 (m, 2H), 10.30 (m, 2H), 9.87 (m, 2H), 8.90-8.48 (m, 7H), 8.26-7.99 (m, 10H), 7.81-7.55 (m, 7H), 4.73 (m, 6H), 1.84 (m, 4H). HRMS TOF : Calcd for $C_{52}H_{44}N_8O_4^{2+}$ $[M-2I]^{2+}$: 844.3475 ; found 844.3486

E

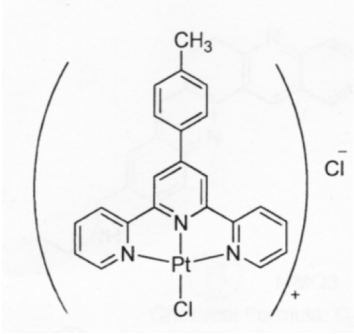

Pt-ttpy
(Bertrand et al., 2007)

F

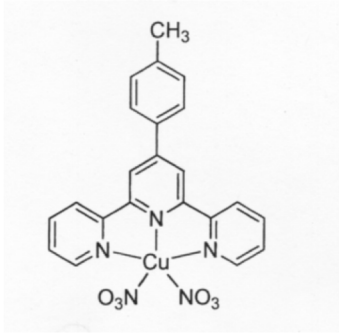

Cu-ttpy
(Bertrand et al., 2007)

Figure S2 Characterization and synthesis of the four newly developed compounds (A-D) and two known compound (E, F) used in the study

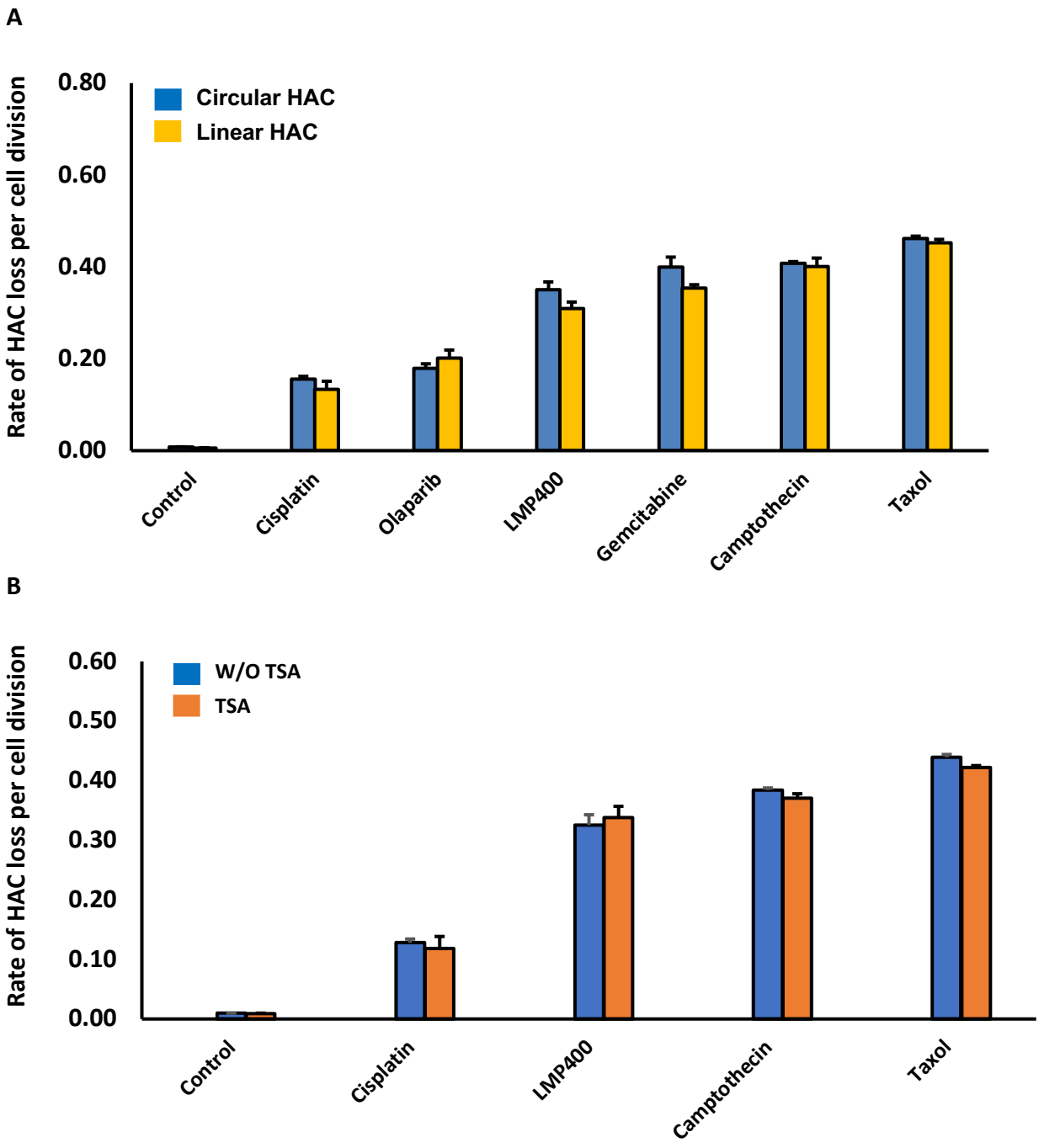

Figure S3 Effect of drugs on HAC mis-segregation rate. **A,** HT1080 cells containing either a circular or a linear HAC were treated by either Taxol or one of the DNA damage compounds, i.e. Camptothecin, Gemcitabine, LMP400, Olaparib and Cisplatin. The rate of HAC loss (a linear versus circular HAC) per cell division was calculated based on the ratio of HAC-positive, HAC-negative, and the average time per cell division. The drugs concentrations used were at LC50 for HT1080 cells (18). The control corresponds to the frequency of spontaneous loss of the EGFP-HACs in human HT1080 cells. **B,** Treatment of HT1080 cells containing EGFP-alphoid^{tetO}-HAC with the histone deacetylase (HDAC) inhibitor, TSA (trichostatin). As seen, loss of EGFP signal after cells treatment with the Cisplatin, LMP400, Camptothecin and Taxol results from HAC loss but not from the transgene silencing caused by heterochromatinization of the *EGFP* region in the HAC.

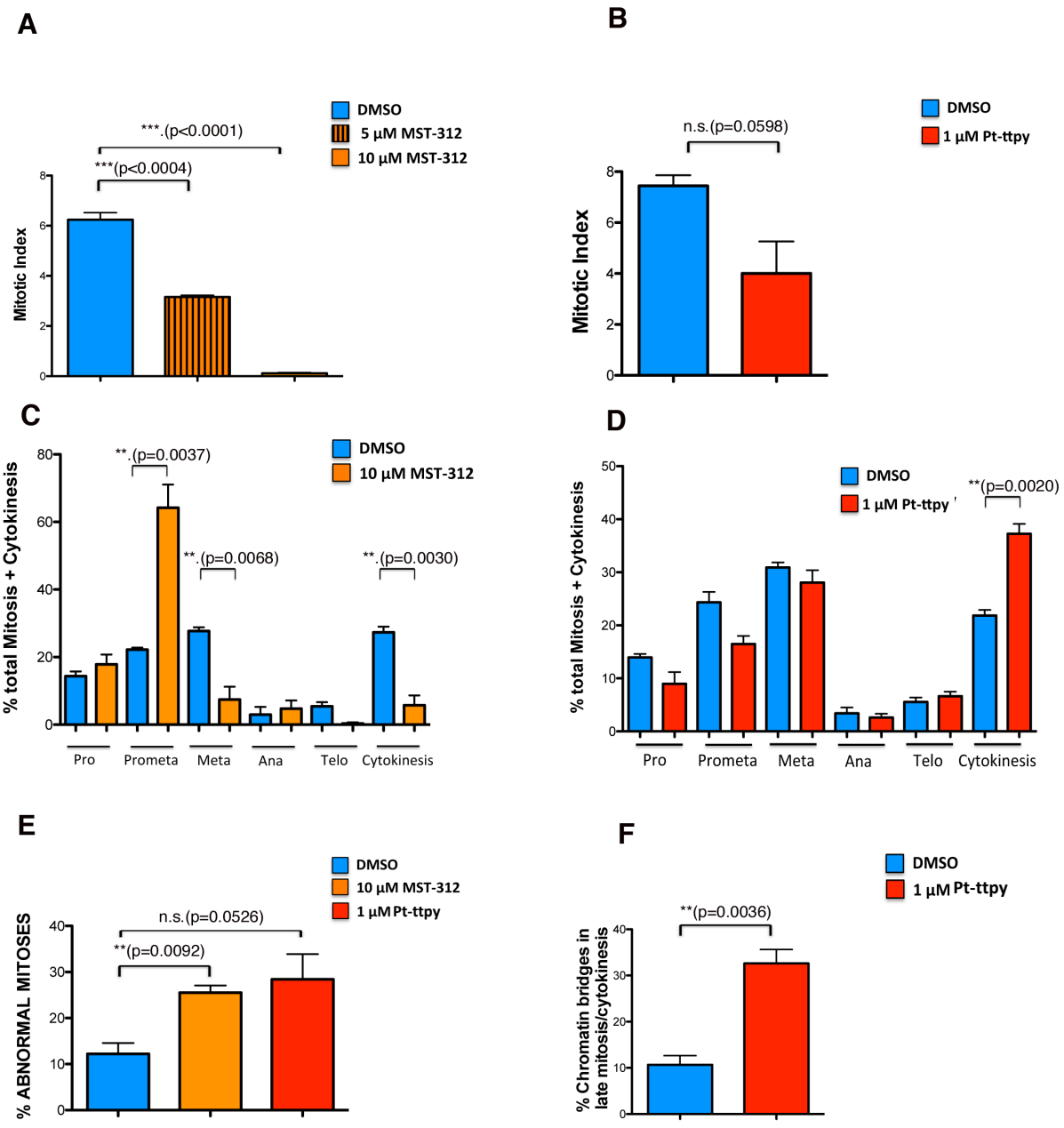

Figure S4 Quantification of defects in mitosis upon Pt-ttpy and MST-312 treatment of HCT116 cells. **A,** Mitotic index (a ratio between the number of cells in a population undergoing mitosis to the total number of cells) upon treatment with DMSO (control), 5 µM and 10 µM MST-312. **B,** Mitotic index upon treatment with DMSO (control) and 1 µM Pt-ttpy. In (**A**) and (**B**) three independent experiments were performed for each concentration of the drug and more than 1,000 cells (n) were screened. **C-D**, Distribution of cells in different stages of mitosis upon (**C**) MST-312 and (**D**) Pt-ttpy treatment. Three independent experiments were performed for each concentration of the drug and more than 100 mitotic cells (n) were screened. **E,** Percentage of cells exhibiting defects in mitosis upon MST-312 and Pt-ttpy treatment. Three independent experiments were performed for each concentration of the drug and more than 100 cells (n) were screened. DMSO - in blue; MST-312 -in orange; Pt-ttpy - in red. **F**, Percentage of chromatin bridges in late mitosis and cytokinesis upon treatment with 1 µM Pt-ttpy, as quantified using LAP2 as a marker. Relevant results from statistical analysis (t tests) are shown for each graph; error bars correspond to SD; N.S.= not significant.

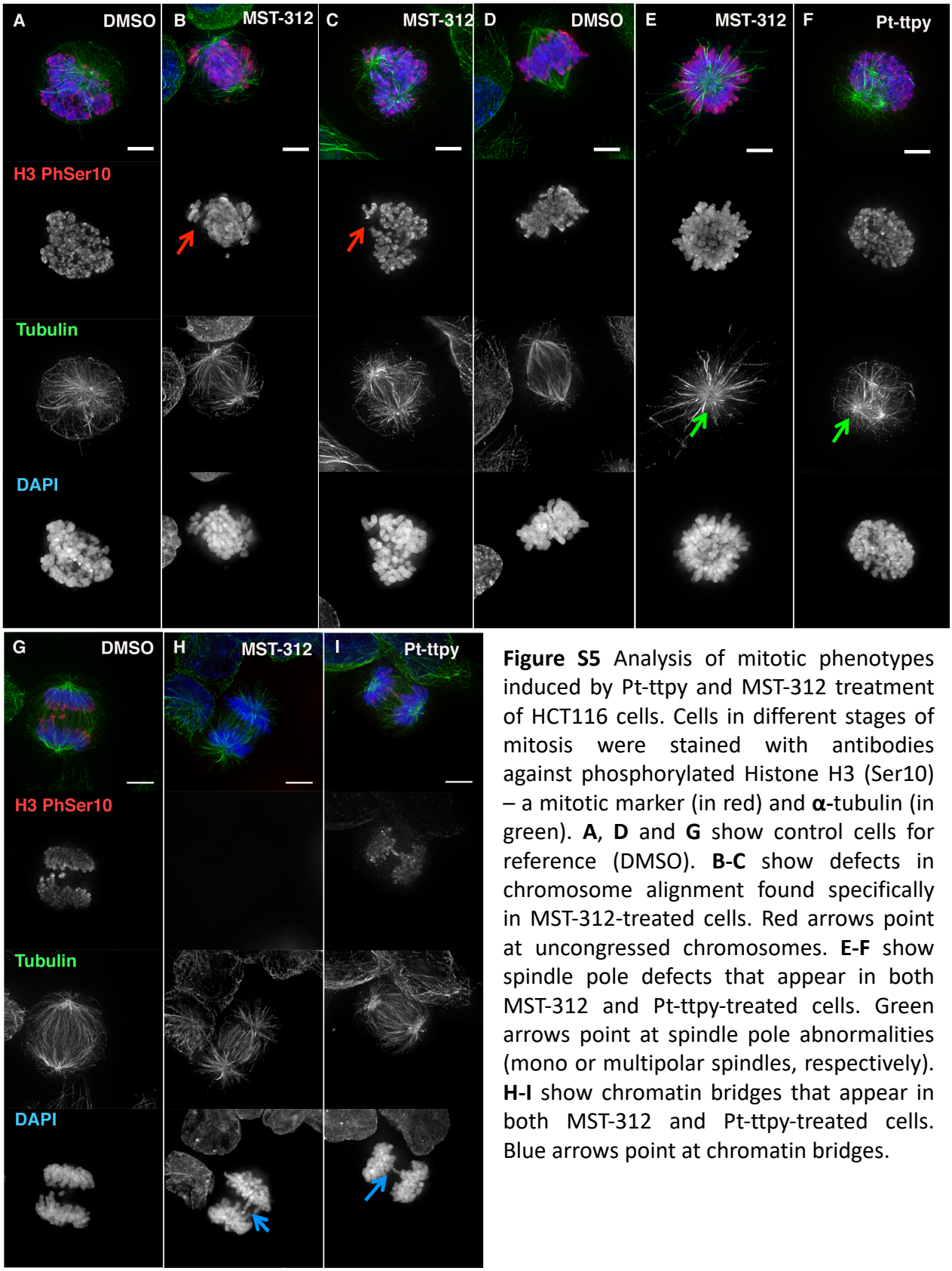

Figure S5 Analysis of mitotic phenotypes induced by Pt-ttpy and MST-312 treatment of HCT116 cells. Cells in different stages of mitosis were stained with antibodies against phosphorylated Histone H3 (Ser10) – a mitotic marker (in red) and **α**-tubulin (in green). **A**, **D** and **G** show control cells for reference (DMSO). **B-C** show defects in chromosome alignment found specifically in MST-312-treated cells. Red arrows point at uncongressed chromosomes. **E-F** show spindle pole defects that appear in both MST-312 and Pt-ttpy-treated cells. Green arrows point at spindle pole abnormalities (mono or multipolar spindles, respectively). **H-I** show chromatin bridges that appear in both MST-312 and Pt-ttpy-treated cells. Blue arrows point at chromatin bridges.

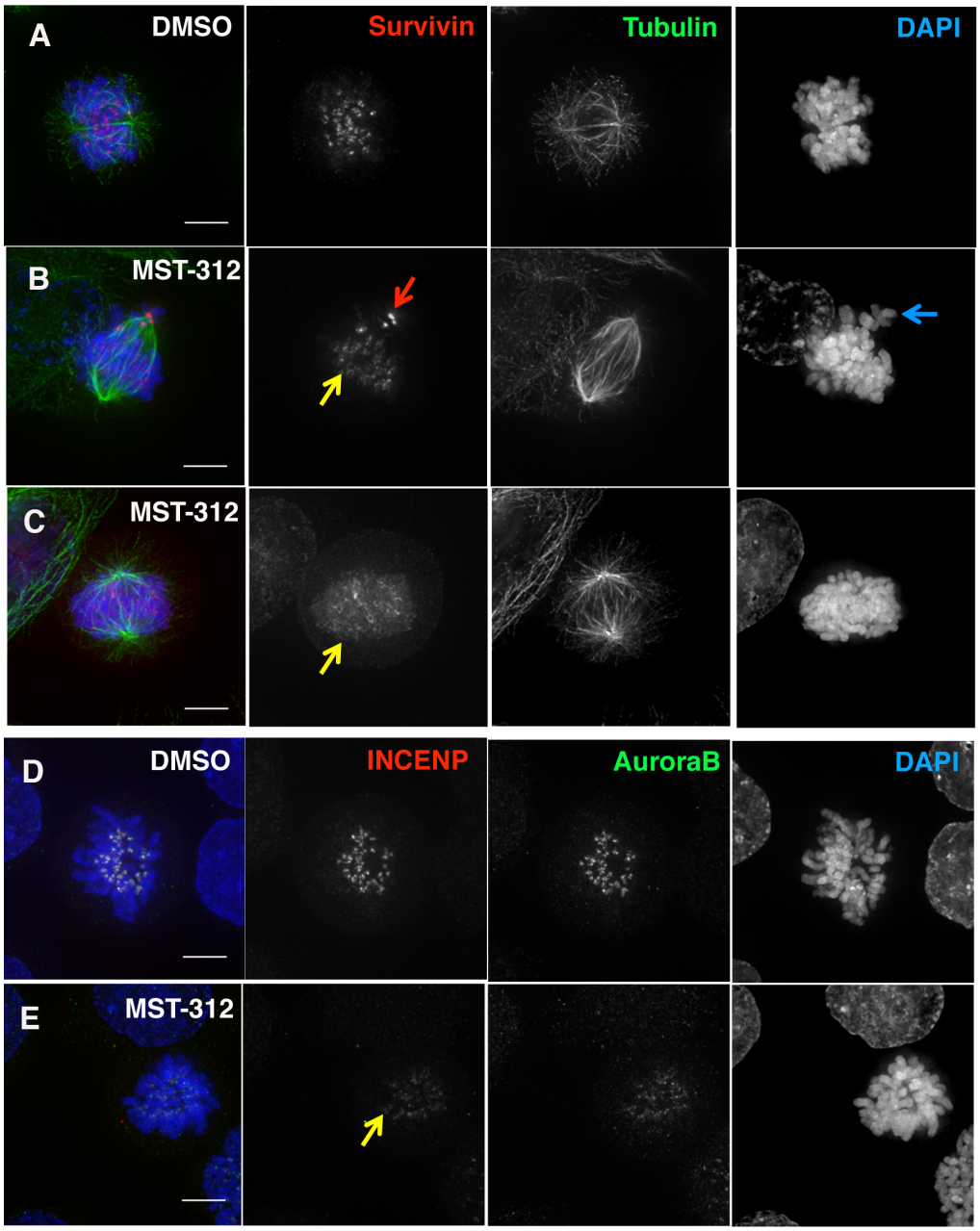

Figure S6 Analysis of the level and localization of the Chromosomal Passenger Complex in early mitosis in MST-312-treated HCT116 cells. **A-C,** Cells were stained with antibodies against Survivin (in red) and **α**-tubulin (in green). Localization of Survivin in (**A**) control cells (DMSO) and (**B-C**) MST-312-treated cells in early mitosis. **D-E,** Cells were stained with antibodies against INCENP (in red) and Aurora B (in green). Localization of INCENP and Aurora B in (**D**) control cells (DMSO) and (**E**) MST-312-treated cells in early mitosis. In drug-treated cells the levels of all three CPC components are lower and the proteins appear to be dispersed along chromosome arms (yellow arrows). Red/blue arrows point to uncongressed chromosomes.

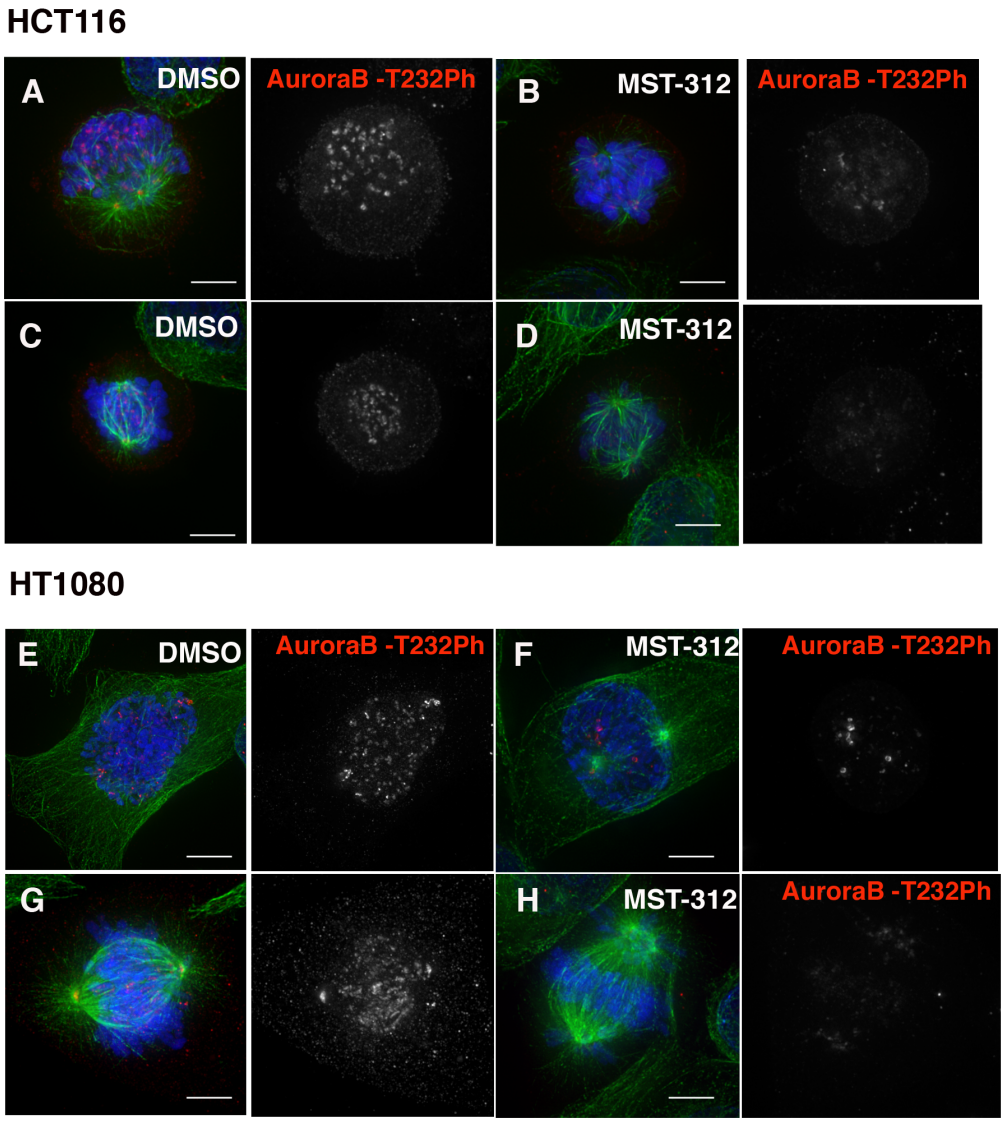

Figure S7 Aurora B kinase activity is reduced in MST-312-treated cells. HCT116 cells (**A-D**) and HT1080 cells (**E-H**) were stained with antibodies against phosphorylated Aurora B (Thr232) (in red) and **α**-tubulin (in green). **A,C,E,G,** Normal localization of phosphorylated Aurora B (Thr232) in control cells (DMSO). **B, D, F, H,** Levels of active Aurora B are reduced in MST-312-treated cells.

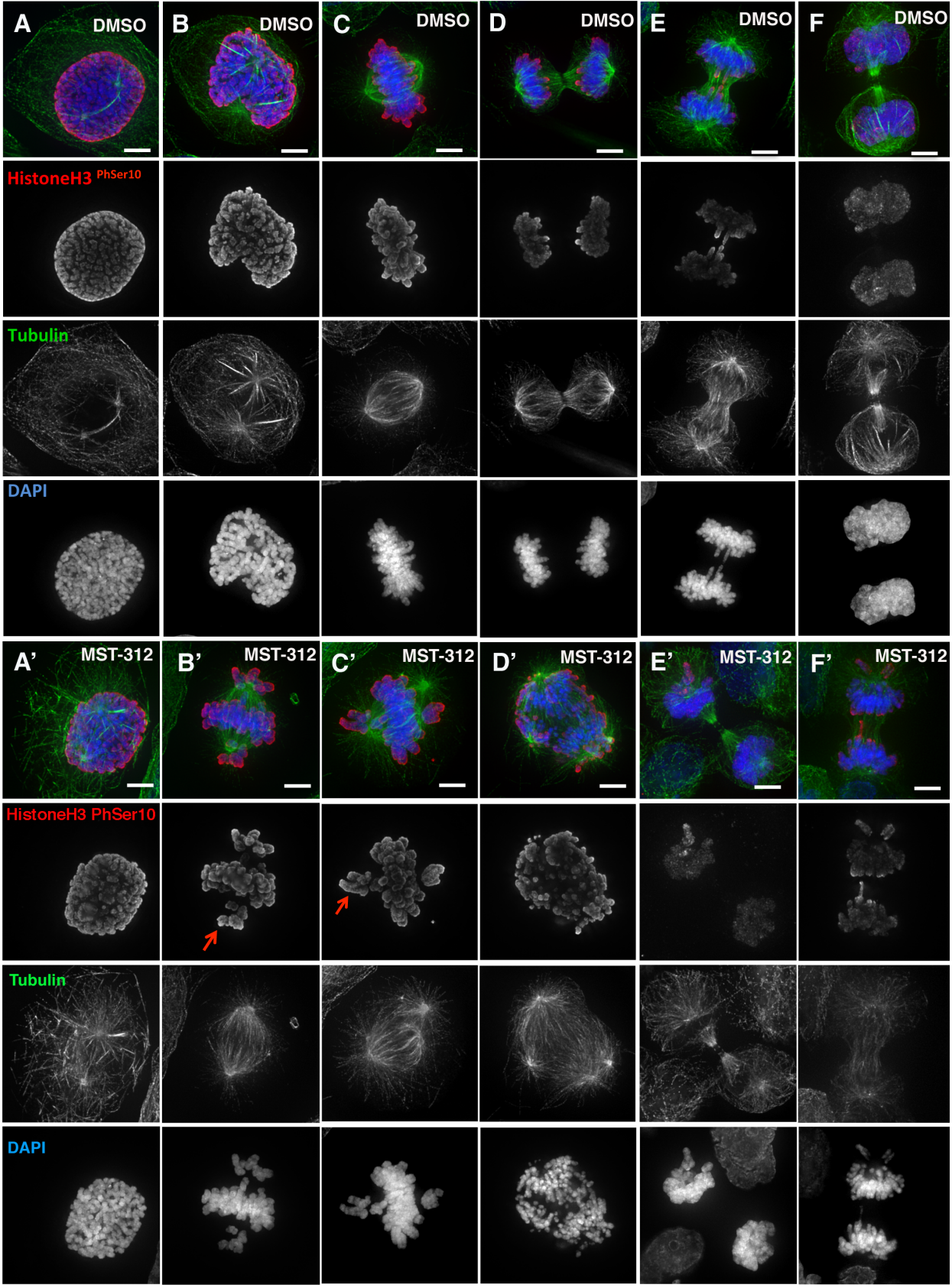

Figure S8 Analysis of mitotic phenotypes induced by MST-312 treatment of U2OS cells. Cells in different stages of mitosis were stained with antibodies against phosphorylated HistoneH3 (PhSer10) –a mitotic marker (in red) and **α**-tubulin (in green). **A-F,** DMSO-treated control cells. **A'-F',** Drug-treated cells. **B'-C',** Chromosome alignment defects in MST-312-treated cells. Red arrows point at uncongressed chromosomes **E'-F',** Absence of chromatin bridges in MST-312-treated cells.

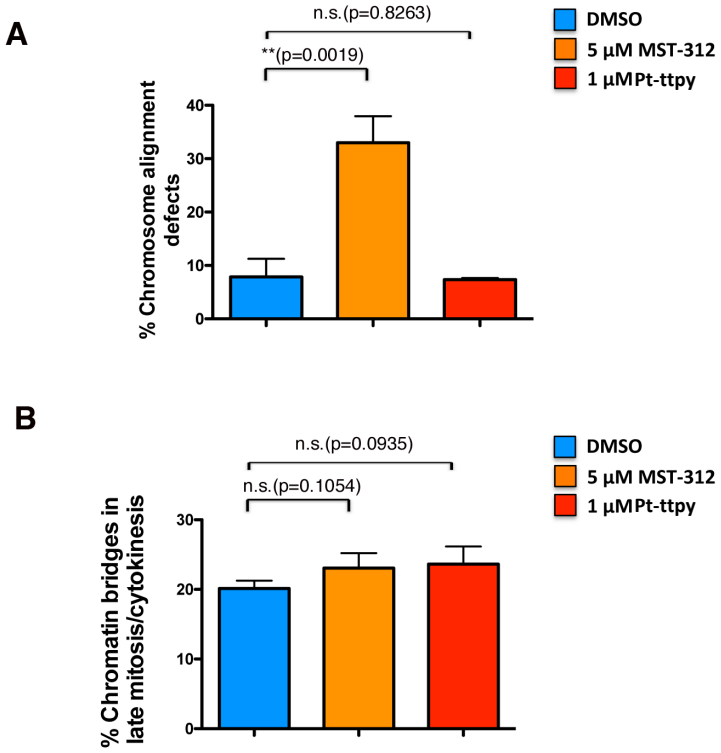

Figure S9 Quantification of mitotic defects in MST-312 and Pt-ttpy-treated U2OS cells. **A,** Quantification of chromosome alignment defects. **B,** Quantification of chromatin bridges in late mitosis and cytokinesis, quantified using LAP2 as a marker. Bars compare results of untreated cells (DMSO) with correspondent drug-treated cells. Relevant results from statistical analysis (t tests) are shown; error bars correspond to SD; N.S.= not significant.

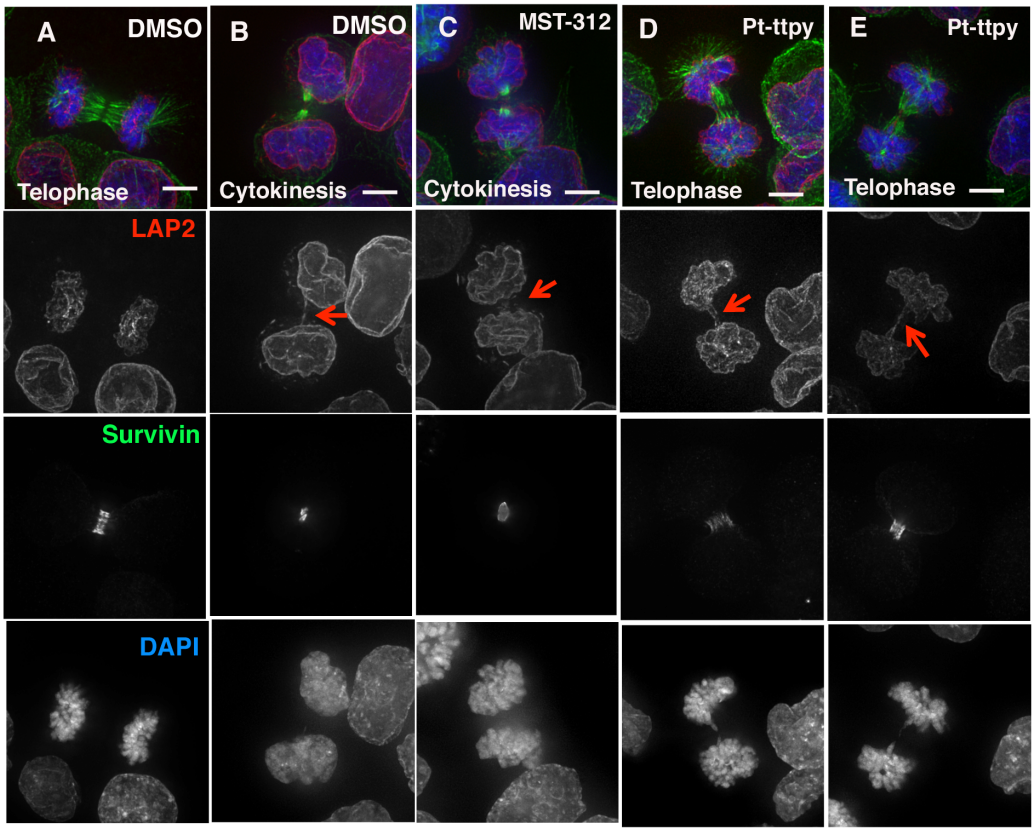

Figure S10 Pt-ttpy and MST-312 treatment generates chromatin bridges in late mitosis. HCT116 cells in different stages of mitosis were stained with antibodies against LAP2 (in red) and **α**-Survivin (in green). LAP2 allows us to visualize and quantify chromatin bridges that are too thin to be spotted with just DAPI staining. **A-B,** DMSO (control cells); **C,** MST-312-treated cells. **D-E**, Pt-ttpy-treated cells. Red arrows point to chromatin bridges.

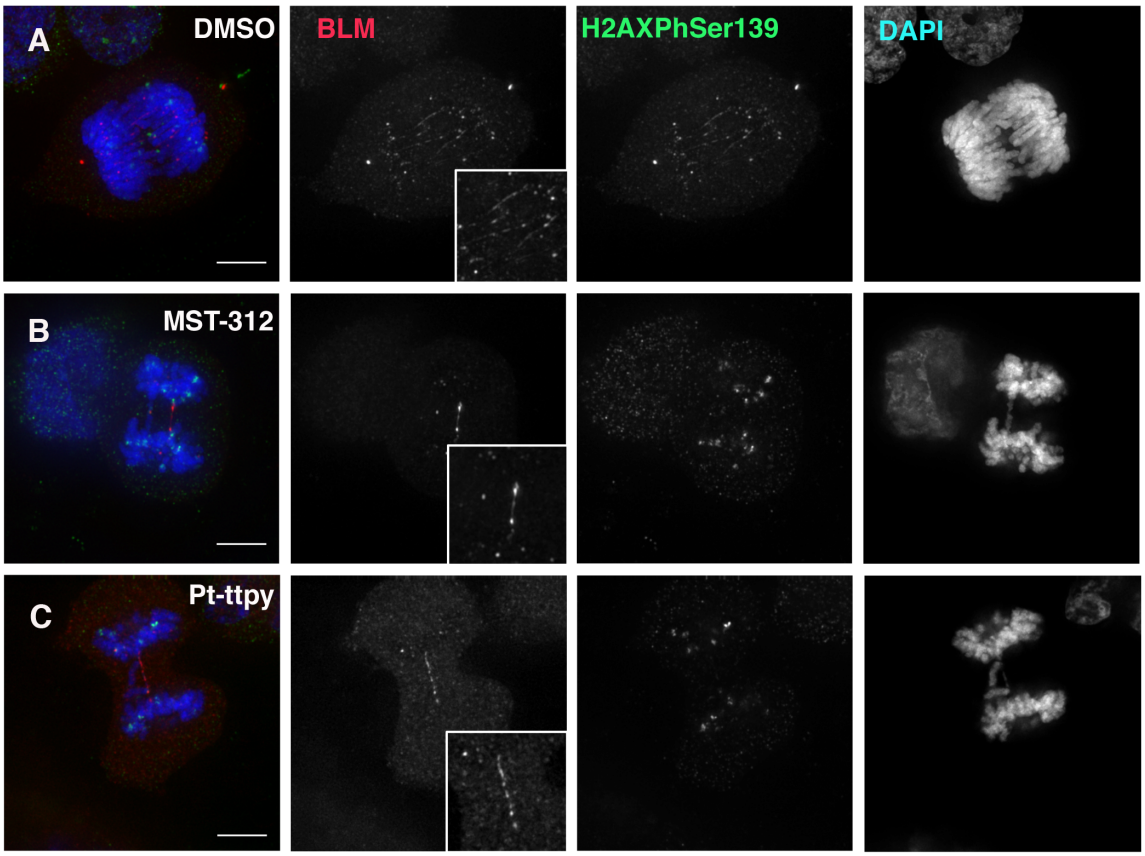

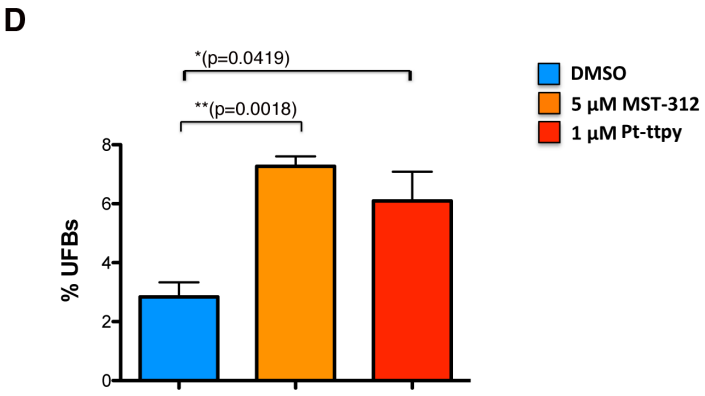

Figure S11 MST-312 and Pt-ttpy treatment increases the frequency of Ultrafine Bridges (UFBs) in HCT116 cells. The cells were stained with antibodies against Blooms Syndrome protein – BLM (in red) and phosphorylated γHistone2AX (in green). Examples of UFBs in control untreated cells (DMSO) (**A**), MST-312-treated cells (**B**) and Pt-ttpy -treated cells (**C**). **D,** Quantification of the percentages of UFBs. Bars compare results of untreated cells (DMSO) with correspondent drug-treated cells. Relevant results from statistical analysis (t tests) are shown; error bars correspond to SD.

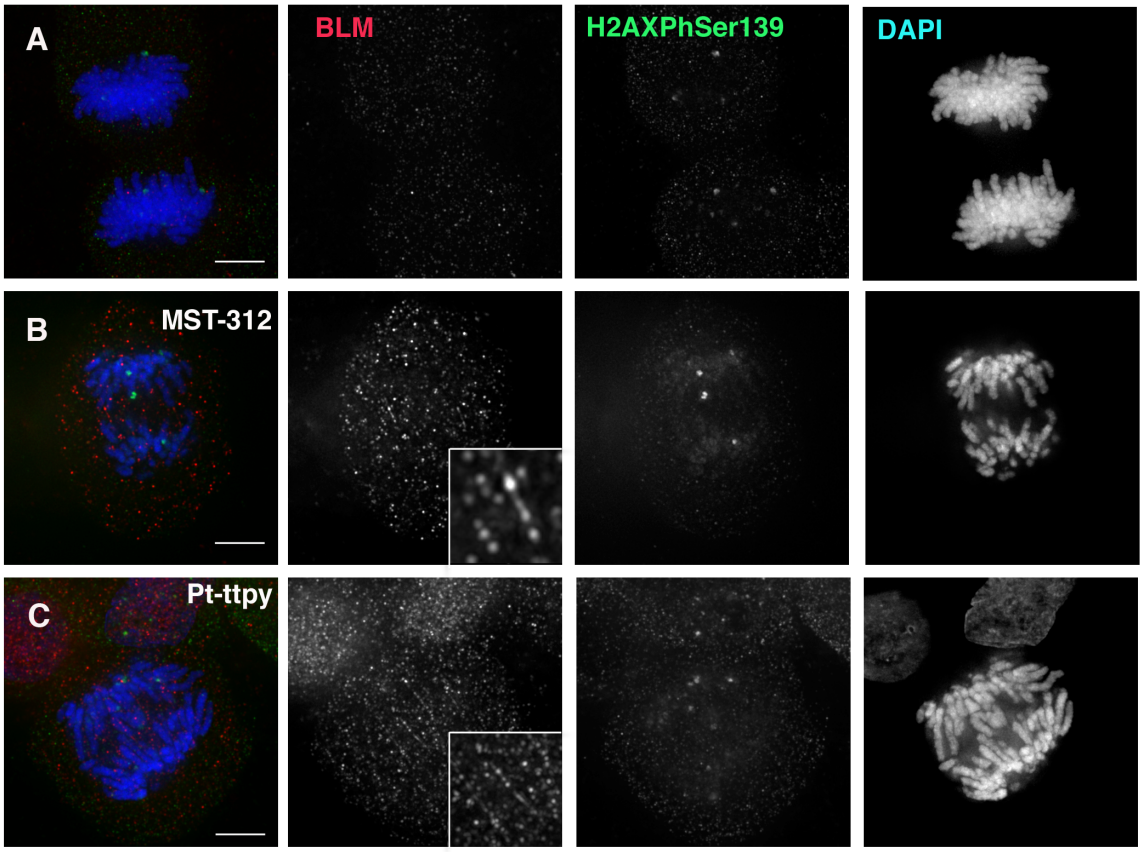

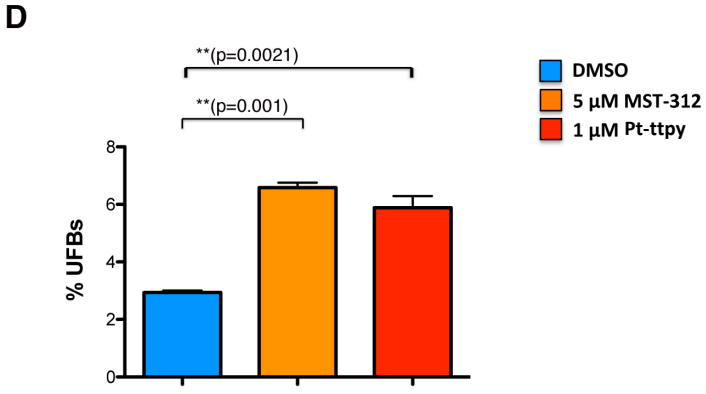

Figure S12 MST-312 and Pt-ttpy treatment increases the frequency of Ultrafine Bridges (UFBs) in HT1080 cells. The cells were stained with antibodies against Blooms Syndrome protein – BLM (in red) and phosphorylated γHistone2AX (in green). Examples of UFBs in control untreated cells (DMSO) **(A**), MST-312-treated cells **(B)** and Pt-ttpy -treated cells **(C)**. **D,** Quantification of the percentages of UFBs. Bars compare results of untreated cells (DMSO) with correspondent drug-treated cells. Relevant results from statistical analysis (t tests) are shown; error bars correspond to SD.

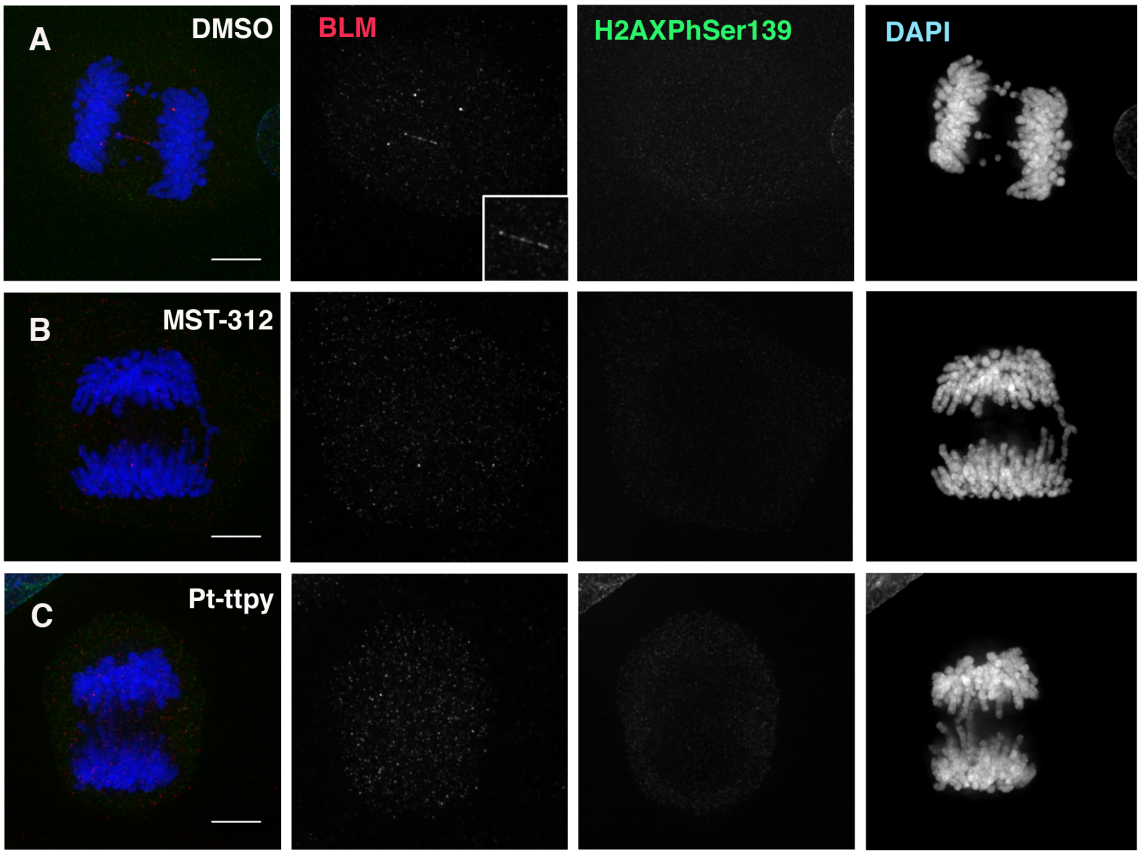

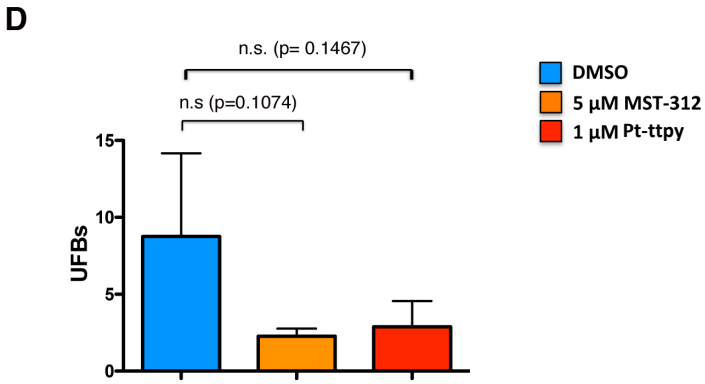

Figure S13 MST-312 and Pt-ttpy treatment does not increase the frequency of Ultrafine Bridges (UFBs) in U2OS cells. Cells were stained with antibodies against Blooms Syndrome protein – BLM (in red) and phosphorylated γHistone2AX (in green). Examples of UFBs in control untreated cells (DMSO) **(A**), absence of UFBs in MST-312-treated cells **(B)** and Pt-ttpy -treated cells **(C)**. **D,** Quantification of the percentages of UFBs in mitotic cells. Bars compare results of untreated cells (DMSO) with correspondent drug-treated cells. Relevant results from statistical analysis (t tests) are shown; error bars correspond to SD. N.S.= not significant.

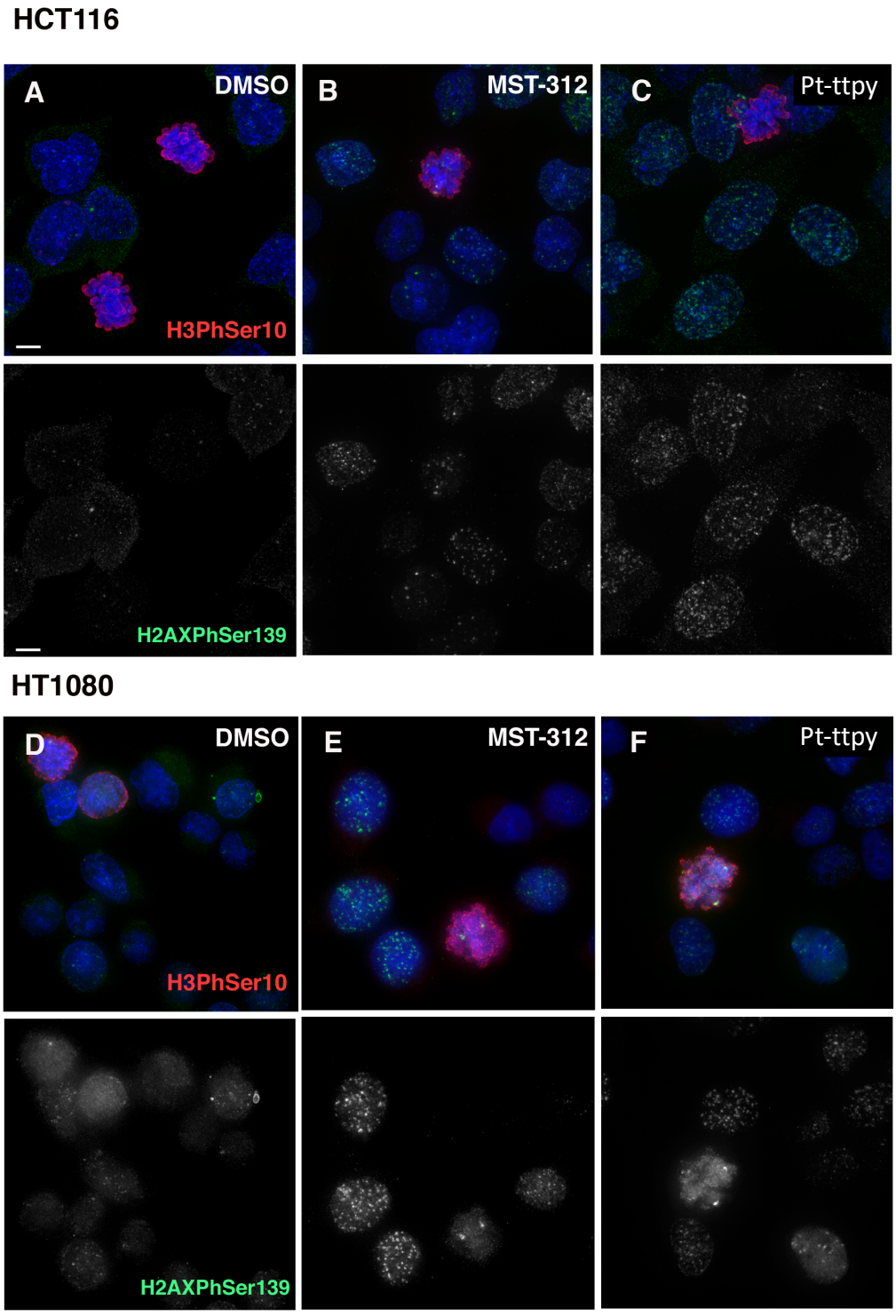

Figure S14 Detection of DSBs after drug treatment in (**A-C**) HCT116 cells and (**D-F**) HT1080 cells. Cells were stained with antibodies against phosphorylated HistoneH3 (Ser10) –a mitotic marker (in red) and phosphorylated γHistone2AX (in green). (**A** and **D**) DMSO control cells; (**B** and **E**) MST-312 and (**C** and **F**) Pt-ttpy -treated cells.

Supplementary Table S1 Drugs used in this study

Drugs	Targeting	Description	Reference
GRN163L	hTERT	Targeting RNA template of telomerase	(55,56)
BIBR1532	hTERT	Small molecule inhibitors	(37*,57)
MST-312	hTERT	Small molecule inhibitors	(58)
6-Thio-dG	hTERT	A nucleoside analogue of telomerase substrate	(36*,47*)
PIPER	G-Quadruplex	Blocking telomerase access to telomeres	(69)
Phen-DC3	G-Quadruplex	Blocking telomerase access to telomeres	(60)
Phen-DC6	G-Quadruplex	Blocking telomerase access to telomeres	(60)
Tris Q	G-Quadruplex	Blocking telomerase access to telomeres	(61)
PhenDC3 C4Bn	G-Quadruplex	Blocking telomerase access to telomeres	This study
Phen DV	G-Quadruplex	Blocking telomerase access to telomeres	(62)
CN1	G-Quadruplex	Blocking telomerase access to telomeres	(63)
Phen DC3 Bisalk1	G-Quadruplex	Blocking telomerase access to telomeres	This study
PDC	G-Quadruplex	Blocking telomerase access to telomeres	(64)
PDC C4Bn	G-Quadruplex	Blocking telomerase access to telomeres	(65)
CuBisQ	G-Quadruplex	Blocking telomerase access to telomeres	(66)
Pt-ttpy	G-Quadruplex	Blocking telomerase access to telomeres	(20*)
Cu-ttpy	G-Quadruplex	Blocking telomerase access to telomeres	(20*,21*)
BRACO 19	G-Quadruplex	Blocking telomerase access to telomeres	(67)
Pyridostatin	G-Quadruplex	Blocking telomerase access to telomeres	(68)
TMPyP4	G-Quadruplex	Blocking telomerase access to telomeres	(69,70)

Bisphenyl VPy	G-Quadruplex	Blocking telomerase access to telomeres	This study
MMQ3	G-Quadruplex	Blocking telomerase access to telomeres	(71)
PhenDV-An	G-Quadruplex	Blocking telomerase access to telomeres	This study

Taxol	Tubulin	Microtubule stabilizing	(18)
LMP400	Top I	DNA damage response/replication	(18)
Gemcitabine	dNTP synthesis	DNA damage response/replication	(18)
Camptothecin	Top I	DNA damage response/replication	(18)
BMN673	PARP	DNA damage response/replication	(18)
Olaparib	PARP	DNA damage response/replication	(18)
Cisplatin	DNA	DNA damage response/replication	(18)

* References presented in the main text.

55. Hochreiter AE, Xiao H, Goldblatt EM, Gryaznov SM, Miller KD, Badve S*, et al.* Telomerase template antagonist GRN163L disrupts telomere maintenance, tumor growth, and metastasis of breast cancer. Clin Cancer Res **2006**;12:3184-92

56. Goldblatt EM, Gentry ER, Fox MJ, Gryaznov SM, Shen C, Herbert BS. The telomerase template antagonist GRN163L alters MDA-MB-231 breast cancer cell morphology, inhibits growth, and augments the effects of paclitaxel. Mol Cancer Ther **2009**;8:2027-35

57. Shi Y, Sun L, Chen G, Zheng D, Li L, Wei W. A combination of the telomerase inhibitor, BIBR1532, and paclitaxel synergistically inhibit cell proliferation in breast cancer cell lines. Target Oncol **2015**;10:565-73

58. Fatemi A, Safa M, Kazemi A. MST-312 induces G2/M cell cycle arrest and apoptosis in APL cells through inhibition of telomerase activity and suppression of NF-kappaB pathway. Tumour Biol **2015**;36:8425-37

59. Kerwin SM, Chen G, Kern JT, Thomas PW. Perylene diimide G-quadruplex DNA binding selectivity is mediated by ligand aggregation. Bioorg Med Chem Lett **2002**;12:447-50

60. Piazza A, Boule JB, Lopes J, Mingo K, Largy E, Teulade-Fichou MP*, et al.* Genetic instability triggered by G-quadruplex interacting Phen-DC compounds in Saccharomyces cerevisiae. Nucleic Acids Res **2010**;38:4337-48

61. Bertrand H, Granzhan A, Monchaud D, Saettel N, Guillot R, Clifford S*, et al.* Recognition of G-quadruplex DNA by triangular star-shaped compounds: with or without side chains? Chemistry **2011**;17:4529-39

62. Beauvineau C, Guetta C, Teulade-Fichou MP, Mahuteau-Betzer F. PhenDV, a turn-off fluorescent quadruplex DNA probe for improving the sensitivity of drug screening assays. Org Biomol Chem **2017**;15:7117-21

63. Halder R, Riou JF, Teulade-Fichou MP, Frickey T, Hartig JS. Bisquinolinium compounds induce quadruplex-specific transcriptome changes in HeLa S3 cell lines. BMC Res Notes **2012**;5:138

64. De Cian A, Delemos E, Mergny JL, Teulade-Fichou MP, Monchaud D. Highly efficient G-quadruplex recognition by bisquinolinium compounds. J Am Chem Soc **2007**;129:1856-7

65. Verga D, Hamon F, Poyer F, Bombard S, Teulade-Fichou MP. Photo-cross-linking probes for trapping G-quadruplex DNA. Angew Chem Int Ed Engl **2014**;53:994-8

66. Largy E, Hamon F, Rosu F, Gabelica V, De Pauw E, Guedin A*, et al.* Tridentate N-donor palladium(II) complexes as efficient coordinating quadruplex DNA binders. Chemistry **2011**;17:13274-83

67. Burger AM, Dai F, Schultes CM, Reszka AP, Moore MJ, Double JA*, et al.* The G-quadruplex-interactive molecule BRACO-19 inhibits tumor growth, consistent with telomere targeting and interference with telomerase function. Cancer Res **2005**;65:1489-96

68. McLuckie KI, Di Antonio M, Zecchini H, Xian J, Caldas C, Krippendorff BF*, et al.* G-quadruplex DNA as a molecular target for induced synthetic lethality in cancer cells. J Am Chem Soc **2013**;135:9640-3

69. Perez-Arnaiz C, Busto N, Santolaya J, Leal JM, Barone G, Garcia B. Kinetic evidence for interaction of TMPyP4 with two different G-quadruplex conformations of human telomeric DNA. Biochim Biophys Acta **2018**;1862:522-31

70. Zheng XH, Nie X, Liu HY, Fang YM, Zhao Y, Xia LX. TMPyP4 promotes cancer cell migration at low doses, but induces cell death at high doses. Sci Rep **2016**;6:26592

71. Hounsou C, Guittat L, Monchaud D, Jourdan M, Saettel N, Mergny JL*, et al.* G-quadruplex recognition by quinacridines: a SAR, NMR, and biological study. ChemMedChem **2007**;2:655-66

Supplementary Table S2 Concentrations of compounds used in this study

Compound	**LC50 in HT1080** (HAC loss)
Phen-DC3	60 μM
Phen-DC6	60 μM
TrisQ	60 μM
PhenDC3-C4Bn	80 μM
PhenDV	80 μM
GRN163L	1-50 μM
CN1	50 μM
Phen-DC3 Bisalk1	50 μM
PDC	50 μM
PDC-C4Bn	50 μM
CuBisQ	80 μM
Pt-ttpy	5 μM
Cu-ttpy	1 μM
Bisphenyl-Vpy	80 μM
MMQ3	100 nM
TMPyP4	80 μM
BRACO19	6 μM
PIPER	100 μM
Pyriostatin	8 μM
BIBR1532	300 μM
MST-312	100 μM
6-Thio-dG	300 μM
PhenDV-An	10 μM
Compound	**Concentration of drugs used to study mitotic abnormalities in HT1080, HCT116, U2OS***

Cu-ttpy	1-2 μM
Pt-ttpy	1-2 μM
MST-312	5-10 μM

***References**

72. Morais KS, Guimarãesb AFR, Ramos DAR, Silva FP, de Oliveira DM. Long-term exposure to MST-312 leads to telomerase reverse transcriptase overexpression in MCF-7 breast cancer cells. bAnticancer Drugs **2017**;28:750-756

73. Wang Y, Sun C, Mao A, Zhang X, Zhou X, Wang Z, Zhang H. Radiosensitization to X-ray radiation by telomerase inhibitor MST-312 in human hepatoma HepG2 cells. Life Sciences **2015;**123:43-50

74. Gurung RL, Lim SN, Low GK, Hande MP. MST-312 Alters Telomere Dynamics, Gene Expression Profiles and Growth in Human Breast Cancer Cells. J Nutrigenet Nutrigenomics **2014**;7:283-298

75. Saker L, Ali S, Masserot C, Kellermann G, Poupon J, Teulade-Fichou MP, Ségal-Bendirdjian E, Bombard S. Platinum Complexes Can Bind to Telomeres by Coordination. Int J Mol Sci **2018**;19(7)